

A multiplexed control architecture for superconducting qubits with row-column addressing

Peng Zhao^{1,2,*}

¹Tongling, Anhui 244000, China

²Beijing Academy of Quantum Information Sciences, Beijing 100193, China

(Dated: March 7, 2024)

In state-of-the-art superconducting quantum processors, each qubit is controlled by at least one control line that delivers control pulses generated at room temperature to qubits at millikelvin temperatures. This strategy has been successfully applied to control hundreds of qubits but is unlikely to be scalable to control thousands of qubits, let alone millions or even billions of qubits needed in fault-tolerance quantum computing. The reason for this is due to the wiring challenge, the number of accommodated control lines is limited by factors, such as the cooling power and physical space of the cryogenic system, the control footprint area at the qubit chip level, and so on. Here, we introduce a multiplexed control architecture for superconducting qubits with two types of shared control lines, row and column lines, providing an efficient approach for parallel controlling N qubits with $O(\sqrt{N})$ control lines. With the combination of the two-type shared lines, unique pairs of control pulses are delivered to qubits on each row-column intersection, enabling parallel qubit addressing. Of particular concern here is that, unlike traditional gate schemes, both single- and two-qubit gates are implemented with pairs of control pulses. Considering the inherent parallelism and the control limitations, the integration of the architecture into quantum computing systems should be tailored as much as possible to the specific properties of the quantum circuits to be executed. As such, the architecture could be scalable for executing structured quantum circuits, such as quantum error correction circuits.

I. INTRODUCTION

To perform quantum computing with noisy qubits for solving valuable problems that are intractable for classical computing, quantum error correction (QEC) is widely recognized as the ultimate solution [1, 2]. To date, among various candidate quantum systems for realizing QEC, superconducting qubits have been demonstrated as a leading one [3–7]. In a superconducting quantum processor with tens of qubits, a recent experiment has shown that QEC begins to suppress logical errors with increasing system sizes [7]. Nevertheless, to fully utilize the power of QEC, such as surface code [2, 8], in quantum computing, it is generally believed that high-fidelity control over millions or even billions of qubits is required [8, 9].

In state-of-the-art superconducting quantum processors, as shown in Fig. 1(a), each qubit is controlled by at least one control line, which delivers dedicated control pulses generated at room temperature to qubits operating at millikelvin temperatures [10–12]. Thus, for controlling a N -qubit system, both the numbers of control lines (input-output connections, IOs) at room temperature P_{RT} and in the dilution refrigerator P_{cryo} are determined by the IO terminals of the qubit chip P_{chip} , which is scale linearly with the qubit number N , see Fig. 1(b), leading to $P_{RT} = P_{cryo} = P_{chip} \sim O(N)$ [13]. This independent control strategy can provide great flexibility in controlling qubits [12] and is applied to achieve low gate errors across small-scale systems with tens or hundreds of qubits. However, given the heating loads from the lines [11], the non-negligible feature sizes of the cables or IO terminals, and at least one digital-to-analog converter (DAC) per line for qubit control [12], it is not scalable to large-scale systems. This

is the direct manifestation of the wiring challenge in scaling-up quantum processors [13–16], i.e., the number of control lines that can be managed is limited by factors, such as the cooling power and geometric space of the cryogenic system, the control footprint area at the qubit chip level, the overhead of classical electronics and so on. To facilitate a more intuitive understanding of such a challenge, there is an insightful comparison, to deliver a superconducting quantum processor with just a few thousand qubits, the number of control lines or IOs is adequate for controlling one billion transistors in state-of-the-art classical processors [14]. In this sense, the wiring challenges need to be addressed before a large-scale superconducting quantum processor becomes feasible.

To alleviate the wiring challenge in superconducting quantum systems, strategies which aim to reduce the control lines running from room temperature to cryogenic temperature, i.e., achieving $P_{RT} < P_{cryo}$, have been explored [17–25]. One of the most widely studied approaches is the implementation of cryogenic control electronics operated at 4 K [19–24] or 10 mK [23–25], but implementing successful qubit control at scale while achieving ultra-low-power dissipation remains challenging. Additionally, on-chip control electronics have also been explored to reduce the chip IO terminals [19, 26]. However, as the control footprint area at the chip level is limited by qubit size, besides the heating dissipation and the newly added noises, the on-chip integration can increase the complexity of wire routing, especially when scaling up. Therefore, a common view is that only taking these strategies alone is unlikely to address the wiring challenge [14].

Besides the above top-down approaches, one alternative that has emerged from taking a bottom-up perspective is to exploit multiplexed qubit control with shared lines to reduce the line overhead. Such a perspective is extensively explored for semiconductor spin qubits [14, 27–29] and superconducting quantum annealing processors [30, 31]. For superconducting

*Electronic address: shangnigu@sina.com

qubits, the most successful demonstration is the frequency-multiplexed qubit readout [32–34], where a single feedline is shared by several readout circuitries, allowing simultaneous readout of several qubits. However, exploring the multiplexing for qubit control is still in its infancy [35–38]. Unlike the independent qubit control, the multiplexed control will degrade the control flexibility. Thus, to realize quantum computing, generally, new control overhead or hardware components shall be introduced [37, 38]. Most importantly, further demonstrations of these new features that are compatible with high-fidelity qubit control are required.

In this work, we propose a multiplexed control architecture for superconducting qubits with row-column addressing, which could in principle enable parallel control of N qubits with $O(\sqrt{N})$ control lines. With the combination of two types of shared control lines, i.e., row and column lines, unique pairs of control pulses are delivered to qubits or couplers on each row-column intersection, allowing parallel single- or two-qubit gate operations in qubit lattices. Accordingly, we present various single- and two-qubit schemes that are both compatible with the row-column addressing and the existing superconducting qubit technologies (with no new hardware components). Moreover, we show that while the control flexibility is compromised, the inherent parallelism allows the architecture to be well-suited for executing structured quantum circuits, which consist of layers of parallel single- or two-qubit gates across qubit lattices, such as QEC circuits.

We note that very recently, a similar scheme for selectively addressing qubits has also been studied in semiconductor spin qubits [39–41] by using two microwave drives and has been proposed to enable parallel single-qubit gates [39].

The paper is organized as follows. In Sec. II, we first provide an overview of the multiplexed control architecture. Then, in QEC with surface code, we illustrate that the integration of the architecture into quantum computing systems should be tailored to the specific quantum circuits. In Sec. III, we give detailed descriptions of the single- and two-qubit gate schemes that support row-column addressing. In Sec. IV, we discuss the challenges to be faced when scaling up. Finally, in Sec. V, we provide a summary of our study.

II. THE MULTIPLEXED CONTROL ARCHITECTURE WITH ROW-COLUMN ADDRESSING

For controlling two-dimensional (2D) square qubit lattices, Figure 1(c) schematically shows the multiplexed control architecture, which comprises two types of shared control lines, row lines and column lines. The qubits are located on the intersections of the two-type lines, thus each qubit is connected (coupled) to a unique pair of control lines, enabling spatial addressing of qubits. When applying appropriate pulses to each of these shared control lines simultaneously, each qubit can be driven by a unique pair of control pulses through the associated row and column lines, e.g., see Fig. 1(c). As we will discuss in the next section, when the pair of control pulses satisfies certain conditions, single- or two-qubit gate operations can be realized. Thus, this control strategy can be well

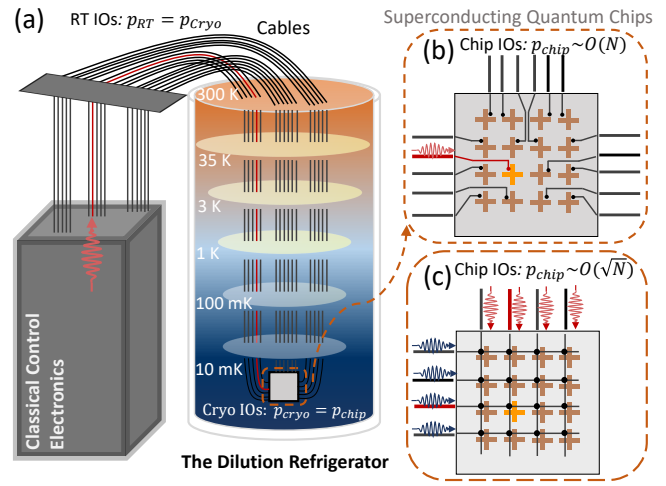


FIG. 1: Schematic (not to scale) of a typical superconducting quantum computing system. (a) Qubits at millikelvin temperatures are controlled by delivering control pulses generated by classical electronics at room temperature through the cables. The number of control lines (input-output connections, IOs) at room temperature P_{RT} and the number of cables in the dilution refrigerator P_{cryo} are determined by the number of input-output (IO) terminals of the chip P_{chip} , leading to $P_{RT} = P_{cryo} = P_{chip}$. (b) With the independent control strategy, $P_{chip} \sim O(N)$, where N is the qubit number. This strategy allows maximum flexibility in controlling qubits, i.e., each qubit (see the qubit highlighted in light orange) can be individually addressed without affecting any other qubits. (c) Within the multiplexed control architecture, by applying appropriate pulses to each of these control lines simultaneously, unique pairs of control pulses are delivered to qubits that are located at the intersection of row lines and column lines, allowing parallel qubit addressing. Hence, the IO terminals P_{chip} scales with \sqrt{N} . Here, each qubit (see the qubit highlighted in light orange) or any subgroup of qubits cannot be individually addressed without affecting all other idle qubits.

suited for performing parallel addressing, allowing simultaneous single- or two-qubit gates across the qubit lattice. Meanwhile, as control lines are shared by qubits, here, each qubit or any subgroup of qubits cannot be selectively addressed without affecting all other idle (inactive) qubits. For example, as shown in Fig. 1(c), when one considers addressing the qubit highlighted in light orange, two pulses are delivered to the associated row and column lines. Thus, idle qubits that are controlled by the same row or column control lines, can be driven by one of the two pulses, causing idling qubit errors.

Evidently, compared to the independent control, there exist two features in controlling qubits. The first feature is that while the multiplexed control can degrade the control flexibility, it is efficient in examining the wiring challenge, allowing parallel control of N qubits with $O(\sqrt{N})$ lines. The second one is that, unlike traditional gate schemes, both single- and two-qubit gates shall be implemented with a pair of control pulses, thus supporting the row-column addressing. Correspondingly, this leads to two issues to be resolved in the architecture, the degradation in control flexibility can affect the usefulness of the multiplexed control in quantum comput-

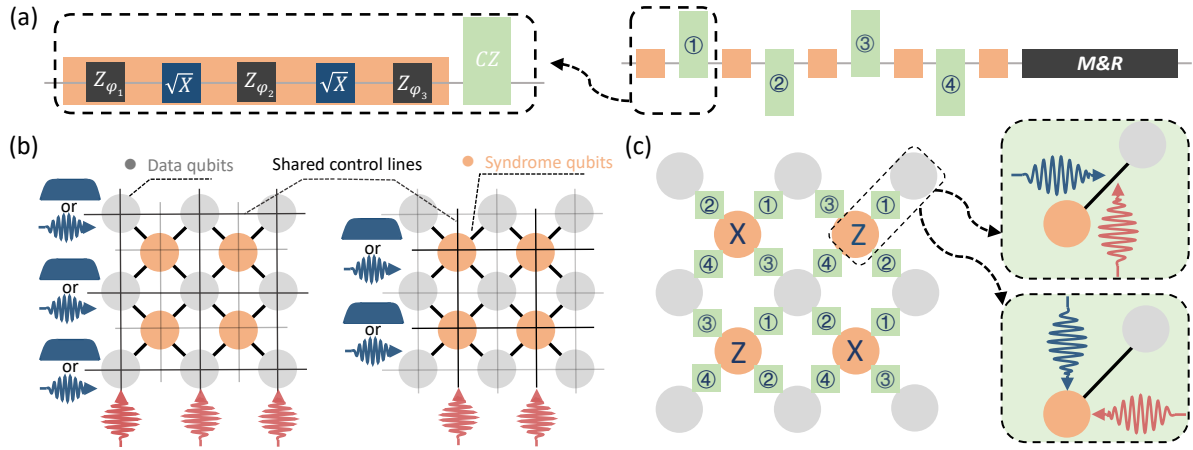


FIG. 2: Multiplexed qubit control for QEC with surface code. (a) A typical stabilizer measurement circuit in surface code using CZ gates, in which the single-qubit gate is further decomposed into two \sqrt{X} gates and three Z gates. During the QEC cycle, interleaved single- and two-qubit gates are implemented and at the end of the cycle, syndrome qubits are measured first and then reset while data qubits are idle. (b) Two sets of shared control lines are employed for independent addressing of data qubits and syndrome qubits. This is adopted to ensure the compatibility between the multiplexed control architecture and the QEC circuits including dynamical decoupling sequences for suppressing qubit idling errors and two-qubit gates with one-qubit driving. Here the shared control lines can deliver microwave pulses or flux pulses for controlling qubits. (c) In QEC with surface code, the order of two-qubit gates depends on the type of syndrome qubits, Z-type or X-type, leading to four different patterns for the sequence of two-qubit gates in the QEC cycle. Hence, for QEC based on two-qubit gates with driven couplers, besides shared lines for qubit addressing, an additional four sets of shared lines are required for selectively choosing gate patterns.

ing, and gate operations supporting the row-column addressing need to be verified. In the following, we aim to first tackle the former one. We will start with a discussion of being agnostic to the physical details of qubits and gate schemes, which will be discussed in the next section.

Although the control flexibility is compromised, the inherent parallelism of the multiplexed control could allow for executing structured quantum circuits, which consist of layers of parallel single- and two-qubit gates across qubit systems (note here that by using the isomorphous waveform technique introduced in Ref. [42], an arbitrary quantum circuit composed of modular single- and two-qubit gates can be compiled into the structured quantum circuits). However, to be practical and useful, the multiplexed control should be tailored to be compatible with the specific properties of the structured circuits.

Here, we consider the realization of a QEC circuit with the multiplexed control scheme. Figure 2(a) shows the typical quantum circuit for stabilizer measurements in surface code using CZ gates [7], in which the single-qubit gate is decomposed into two \sqrt{X} gates and three Z gates [43] (the reason for adopting such decomposition will be discussed in the next section). During the QEC cycle, interleaved single- and two-qubit gates are implemented and at the end of the cycle, syndrome qubits are measured first and then reset while data qubits are idle. To make the control scheme compatible with the QEC circuit, Figure 2(b) shows the multiplexed control architecture comprising two sets of shared row-column lines for independently addressing date qubits and syndrome qubits. This tailored setting is adopted for two reasons: (i) during the syndrome measurement and reset, dynamical decoupling that comprises a sequence of single-qubit gates is generally

applied to data qubits for suppressing idling errors (the idling is currently the dominant error) [7]; (ii) in certain two-qubit gate schemes, only one of the two qubits, e.g., the syndrome qubit shown in the bottom inset of Fig. 2(c), is driven by control pulses [44, 45].

Additionally, in certain two-qubit gate schemes, control pulses are only applied to couplers [46–49], e.g., see the upper inset of Fig. 2(c). Meanwhile, in stabilizer measurement circuits of surface code, the order of two-qubit gates depends on the measured syndromes, Z- or X. This gives rise to four different patterns for the sequence of two-qubit gates in QEC cycles [1, 2], as shown in Fig. 2(c). Therefore, here, besides the shared lines for qubit addressing, an additional four sets of shared lines are required for selectively choosing the gate pattern and addressing couplers in the subgroup of the whole lattice.

Before leaving this section, note that while here we only focus on QEC circuits, we expect that the multiplexed control can also be tailored for logical operations. This is supported by the following three observations. First, logical operations, such as using lattice surgery [50, 51], in essence, involve different patterns of stabilizer measurements [51], which themselves are compatible with the multiplexed control. Second, a more tailored setting can be introduced for patterns of stabilizers that are incompatible with the above setting and the added line overhead can scale with \sqrt{N} . Third, while selectively addressing a few subgroups of qubits, i.e., selecting patterns of stabilizers for logical operations, can result in qubit idling errors, the errors, e.g., phase errors due to off-resonance drives, could be compensated in subsequent QEC cycles.

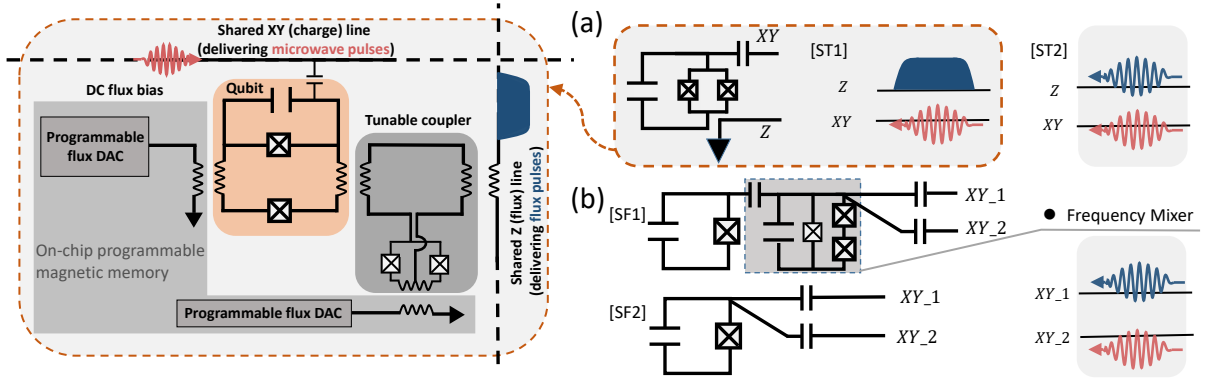


FIG. 3: Schematic illustration of single-qubit gate schemes with two control pulses. (a) Single-qubit gates applied to frequency-tunable transmon qubits. During single-qubit gate operations, a flux pulse and a microwave pulse are simultaneously delivered to the qubit through the Z line and the XY line, respectively. The static DC flux biases are needed for biasing the qubits at their idle points and are realized by using an on-chip programmable magnetic memory, e.g., a Φ -DAC. (ST1) illustrates the gate scheme based on tuning the qubit on-resonance with the microwave drive pulse according to a baseband flux pulse. Individual tuning of the coupling between the Z line and the qubit is achieved by a tunable rf-SQUID coupler, which is biased by a Φ -DAC. (ST2) shows the gate scheme that utilizes the combination of the parametric drive and the microwave drive. Due to the nonlinear dependence of the qubit frequency on the flux bias, the parametric-driven qubit can have a series of sideband frequency components. When one of such sidebands is on-resonance with the microwave drive, qubit control can be achieved. (b) Single-qubit gates for fixed-frequency transmon qubits. During single-qubit gates, a pair of microwave drive pulses are simultaneously delivered to the qubit through the two XY lines. (SF1) depicts the gate schemes using the three-wave mixing process mediated by a flux qubit. When the sum-frequency or difference-frequency of the two microwave drives is on-resonance with the qubit, the qubit can be driven by an effective on-resonance drive. (SF2) displays the gate scheme that uses one off-resonance microwave drive to control a qubit dressed by a second off-resonance drive.

III. GATE OPERATIONS IN THE MULTIPLEXED CONTROL ARCHITECTURE

Here we turn to illustrate how single- and two-qubit gates are realized in the multiplexed control architecture. As shown in Figs. 1(c) and 2, gate operations, unlike that in the conventional independent control scheme, are implemented by applying simultaneous control pulses to all the shared row and column lines. When focusing on one particular qubit or coupler in the lattice, single- and two-qubit gate operations are realized by applying a unique pair of control pulses to a qubit or a coupler. In this section, we propose various gate schemes that are both compatible with the two-pulse configuration and the existing superconducting qubit technologies. For illustration purposes, we focus on the gates applied to transmon qubits [52], but in principle, it should also be feasible for other superconducting qubits, such as fluxonium qubits [53].

A. Single-qubit gates

Table I summarizes four single-qubit gate schemes using two control pulses, which are also schematically illustrated in Fig. 3. The schemes can be grouped into two categories, depending on whether the qubit is tunable. In the following, we shall give detailed descriptions of the four schemes.

Type-ST: This category is for single-qubit gates applied to frequency-tunable qubits. During single-qubit gate operations, a flux pulse and a microwave pulse are simultaneously delivered to the qubit through a shared Z line and a shared

TABLE I: Single-qubit gate schemes with two control pulses. The schematic illustration of these schemes is shown in Fig. 3. Note that for frequency-tunable qubits, static DC flux biases (not listed here, but shown in Fig. 3) are generally needed for biasing the qubits at their idle points.

| Specific | Single-qubit addressing strategy |
|-----------------|-------------------------------------------------------------------------------------------------------|
| Tunable element | (ST1) Baseband flux bias + microwave drive [36, 37]; (ST2) Flux modulation + microwave drive [35]; |
| Fixed element | (SF1) Frequency mixer: e.g. three-wave mixing [54–57]; (SF2) Two-tone microwave drive [58–62]; |

XY line, respectively, as shown in Fig. 3(a). Additionally, for frequency-tunable qubits, static DC flux biases are generally needed for biasing the qubits at their idle points. Following Ref. [30], this flux offset can in principle be introduced by using Φ -DAC, which functions as on-chip programmable magnetic memory, providing the needed static bias. Moreover, the Φ -DAC can be efficiently programmed and addressed by examining the addressing circuitry, which requires $O(\sqrt[3]{N})$ control lines for N frequency-tunable qubits [31].

(ST1) This control scheme comprises a microwave drive pulse and a baseband flux pulse. Similar to Refs. [36, 37], single-qubit gates, such as \sqrt{X} gates, are realized by individually tuning qubits on resonance with the shared microwave drive. However, unlike the previous works using an always-on microwave drive, here a microwave drive pulse is employed (compared to that with the always-on drive [37], this shared

control pulse will not affect other qubit operations, such as qubit readout, qubit reset, and two-qubit gates). Thus the derivative removal by adiabatic gate (DRAG) can be used for realizing single-qubit gates [63]. Accordingly, Figure 4(a) shows the typical two-pulse configuration, which consists of a raised cosine flat-top flux pulse for tuning the qubit frequency from the idle point to the working point and a cosine DRAG pulse for XY control [64]. As qubit idling frequencies should be different from qubits to qubits, the amplitude of the flux pulse applied to each qubit should be individually tuned on resonance with the shared microwave drive. Given that the flux pulse is applied globally to qubits through the shared Z lines, individual tuning can be achieved by realizing tunable coupling between qubits and the shared Z lines. Following Ref. [30], Figure 3(a) shows the tunable rf-SQUID coupler [65–67], which itself is controlled by a Φ -DAC, for individually tuning the amplitudes of flux pulses felt by qubits.

(ST2) This scheme consists of a parametric drive pulse through the Z line and a microwave drive pulse through the XY line. As illustrated in Refs.[35, 45, 68], modulating the qubit frequency with a parametric drive can induce a series of sidebands due to the nonlinear dependence of the qubit frequency on the flux bias. When one of such sidebands is on-resonance with the microwave drive, coherent qubit control can be achieved [35]. Figure 4(b) shows such a pulse configuration, in which a flat-top parametric drive pulse with cosine-shape ramps is used to modulate the qubit frequency and a raised cosine flat-top microwave drive pulse is for XY control. Note that similar schemes have also been studied recently in semiconductor spin qubits [39–41].

Type-SF: This category is for single-qubit gates applied to fixed-frequency qubits. During single-qubit gates, a pair of microwave drive pulses are simultaneously delivered to the qubit through the two XY lines, as shown in Fig. 3(b).

(SF1) Based on an on-chip ‘three-wave mixer’ [54–57], the two microwave drives are converted to an effective qubit drive. When the sum-frequency or difference-frequency of the two drives is on-resonance with the qubit, coherent control of the qubit can be achieved with the effective drive. Figure 3(b) schematically illustrates such an on-chip mixer based on flux qubit [56, 57], which is capacitively coupled to the transmon qubit and is driven by the two microwave drives. Here, for example, we consider that the difference frequency of pulses equals the qubit frequency. Accordingly, Figure 4(c) shows the typical used raised cosine flat-top pulses.

(SF2) Here, single-qubit gates are realized by applying two off-resonance microwave drives to the qubit [58–62], as shown in Fig. 3(b). Such scheme can be understood as follows: one of the two off-resonance drives is used to dress the (bare) qubit and shift the qubit frequency through the ac-Stark effect, while the second one is applied for controlling such microwave-dressed qubit [69–71]. Moreover, this two-tone drive scheme can be combined with the DRAG scheme to suppress leakage errors during gate operations. Figure 4(d) shows the typical used cosine DRAG pulses.

For each of the schemes schematically illustrated in Fig. 3 (also summarized in Table I), Figure 5 presents the numerical verification of their feasibility for performing single-qubit

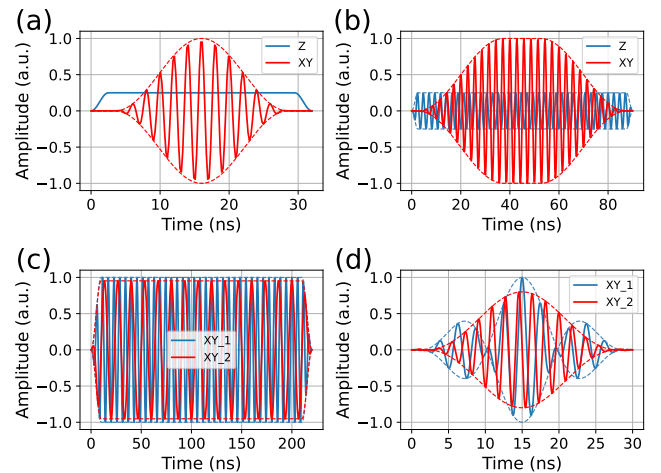


FIG. 4: The control pulses for single-qubit gate schemes schematically illustrated in Fig. 3 (also summarized in Table I). The dashed lines denote the pulse envelopes. (a) shows the pulses for the gate scheme (ST1), using a 25-ns cosine DRAG pulse and a flat-top baseband pulse with a cosine ramp of 2.5 ns. Here, a delay of 1 ns is inserted between the two pulses, giving rise to the total gate length of 32 ns. (b) shows the pulses for the gate scheme (ST2), using a flat-top parametric drive pulse with the ramp time of 2.5 ns and a flat-top microwave drive pulse with the ramp time of 35 ns. The total gate length is 90 ns. (c) shows the pulses for the gate scheme (SF1), using two 220-ns flat-top microwave drive pulses with the same ramp time of 10 ns. (d) shows the pulses for the gate scheme (SF2), using two 30-ns DRAG pulses. Note here that the DRAG coefficient is $\alpha = 1$ for suppressing leakage and only the in-phase component of the cosine DRAG pulse is shown for clarity.

gates, e.g., \sqrt{X} gates or X gates, according to the control pulses shown in Fig. 4. Here, the upper panel shows the population (P_0) in state $|0\rangle$ at the end of the applied pulses with the qubit prepared in its ground state. The dashed grey line denotes the available regions of the control parameters for realizing \sqrt{X} gates while the red star is for X gates. Furthermore, the bottom panel shows the leakage L_1 [72]. These numerical results suggest that low-leakage, high-fidelity single-qubit X rotations can be achieved with the proposed schemes.

As shown in Fig. 2(a), to achieve universal single-qubit control, here we consider compiling arbitrary single-qubit gates into two \sqrt{X} gates and three physical (or virtual) Z gates [43]. The main reason for taking such a compiling method is twofold. First, we prefer the \sqrt{X} gate rather than the X gate due to that the former one can provide more flexibility in choosing control parameters. This could provide possible adaptations to inhomogeneities in coupling efficiencies between qubits and control lines, defects affecting the qubit performance [37], frequency crowding in choosing control frequencies, and so on. Second, as control pulses are shared by qubits, individual Z gate applied to each qubit cannot be directly realized by the phase shift of the shared microwave drive or parametric drive [43, 73], especially in the gate schemes of (ST1), (ST2), and (SF2). Besides the main reason, single-qubit errors, that result from microwave crosstalk,

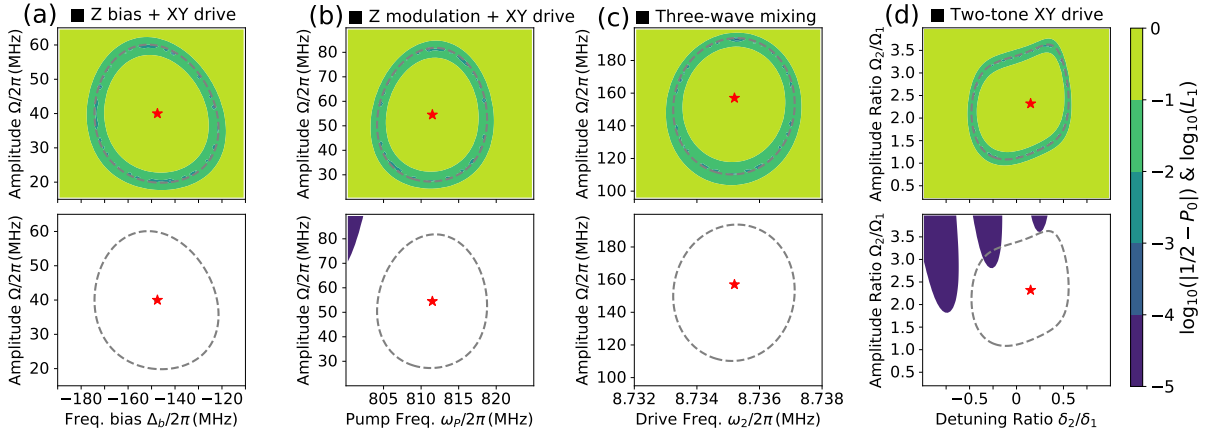


FIG. 5: The numerical verification of the four single-qubit gate schemes. In the numerical analysis, the transmon qubit is treated as an anharmonic oscillator [52] with the (maximum) frequency of $\omega_q/2\pi = 5.25$ GHz and the anharmonicity of $\eta_q/2\pi = -250$ MHz. The upper panel shows the population P_0 at the end of the applied gate pulses shown in Fig. 4 with the qubit prepared in state $|0\rangle$, while the bottom panel is for the leakage L_1 (white regions are where leakage below 10^{-5}). Dashed grey lines indicate the available regions for realizing \sqrt{X} gates while the red star is for X gates. (a) P_0 and L_1 versus the peak drive amplitude Ω of the DRAG pulse (with the frequency of $\omega_d/2\pi = 5.10$ GHz) and the frequency bias $\Delta_b = \omega_q - \omega_d$. (b) P_0 and L_1 versus the parametric drive frequency ω_p and the microwave drive amplitude Ω with the drive frequency of $\omega_d/2\pi = 5.75$ GHz. Here, the dependence of qubit frequency on the flux bias is approximated by $\omega(\Phi) = (\omega_q - \eta_q)\sqrt{|\cos(\pi\Phi/\Phi_0)|} + \eta_q$ [52], where Φ_0 denotes the flux quantum. The used parametric drive is $\Phi = 0.05\Phi_0 + \Phi_p(t)\Phi_0 \cos(\omega_p t + \phi_0)$ (for simplicity, here $\phi_0 = 0$) with the peak drive amplitude $\Phi_p = 0.2$. The result shows the first-order sideband transition with $\omega_p \sim |\omega_d - \omega_q|$. (c) P_0 and L_1 versus the peak drive amplitudes Ω of the two pulses and the frequency of the second drive ω_2 . The frequency of the first drive is $\omega_1/2\pi = 3.5$ GHz. Here, the flux qubit which is treated as a qutrit with the cycle transitions of $(\omega_{01}/2\pi = 6.25$ GHz, $\omega_{02}/2\pi = 10$ GHz, $\omega_{12}/2\pi = 3.75$ GHz) and the transmon-flux coupling strength is $(g_{01}/2\pi = 94$ MHz, $g_{02}/2\pi = 140$ MHz, $g_{12}/2\pi = 136$ MHz) [57]. (d) P_0 and L_1 versus the drive amplitude ratio Ω_2/Ω_1 and the drive-qubit detuning ration δ_2/δ_1 of the two pulses with $\delta_{1(2)} = \omega_{1(2)} - \omega_q$. Here, for the first drive, the peak drive parameters and the drive-qubit detuning are $\Omega_1/2\pi = 15$ MHz and $\delta_1/2\pi = 50$ MHz, respectively.

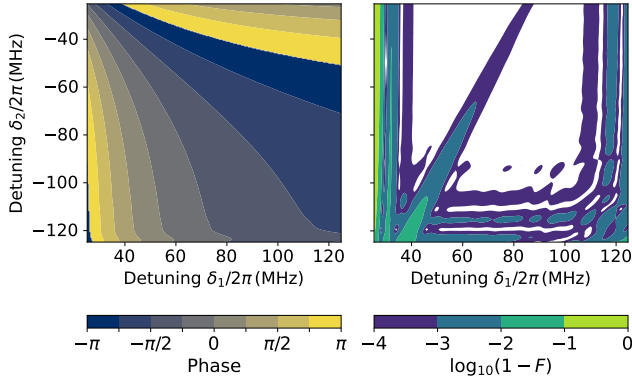


FIG. 6: Single-qubit Z gates. The arbitrary Z gates can be obtained by applying two off-resonance drives. Here, similar to Fig. 4(c), two 150-ns flat-top pulses with a ramp time of 50 ns are utilized. The left panel shows the angles of the Z rotation versus the two drive-qubit detunings δ_1 and δ_2 . The associated Z gate error is shown in the right panel (white regions are where gate errors are below 10^{-4}).

could be mitigated by optimizing the Z gates [74, 75].

For the gate scheme of (SF1) based on the tree-wave mixing process, the phase of the effective drive applied to the

qubit can be controlled by the difference phase or sum phase of the two pulses. Thus, in principle, the virtual Z gates can be utilized here. However, as mentioned above, for the gate schemes of (ST1), (ST2), and (SF2), the physical Z gates are needed. Generally, this can be realized by using the ac-Stark effect resulting from off-resonance microwave drives [76]. Here, we consider the implementation of arbitrary Z gates in (SF2), where two off-resonance microwave drive pulses are applied to the qubit. Similar to Fig. 4(c), a pair of raised cosine flat-top pulses are employed for performing Z rotations. Figures 6(a) and 6(b) show the Z rotation angle and the gate fidelity [77] versus the two drive-qubit detunings, respectively, illustrating that arbitrary Z rotations can be realized with high fidelity. Note here that while similar to the gate scheme of (F1), the phase difference can be controlled, the nonlinear dependence of the qubit dynamics on the frequency difference or phase difference makes it incompatible with the virtual Z scheme [58], see Appendix A for details.

B. Two-qubit gates

As discussed in Sec. II, to be compatible with the multiplexed control architecture, we consider two-qubit gates based on driving single qubit or a coupler in two-coupled qubit systems. Accordingly, Table II summarizes three possible two-

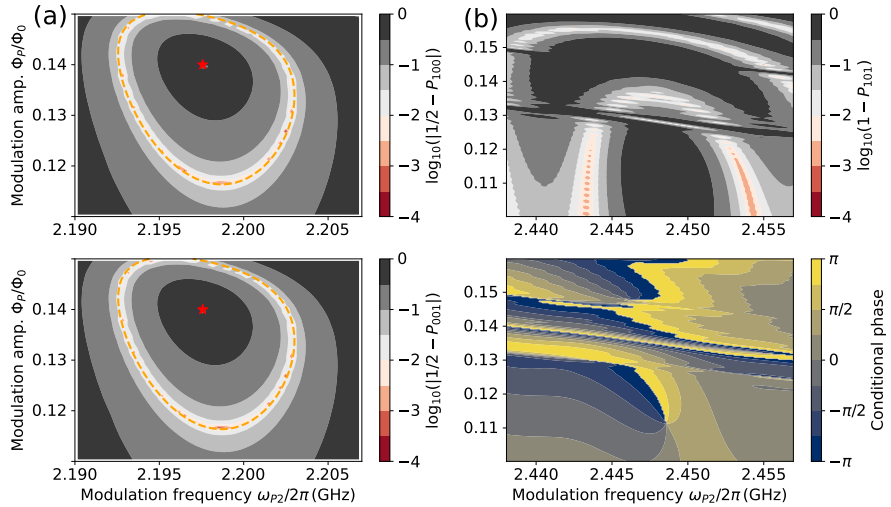


FIG. 7: The numerical verification of the two-qubit gate operations based on two-tone flux modulations. In the numerical analysis, we consider that two transmon qubits (labeled by Q_a and Q_b) are coupled via a tunable bus (labeled by Q_{bus}), and the system state is denoted by $|Q_a Q_{bus} Q_b\rangle$. The qubit frequencies are $\omega_{a(b)}/2\pi = 5.05(5.25)$ GHz and the qubit anharmonicity is $\eta_{a(b)}/2\pi = -250$ MHz. The maximum frequency and the anharmonicity of the tunable bus are $\omega_{bus}/2\pi = 6.20$ GHz and $\eta_{bus}/2\pi = -200$ MHz, respectively. The qubit-bus coupling strength is $g/2\pi = 100$ MHz. The dependence of bus frequency on the two-tone flux modulation is approximated by $\omega_{bus}(\Phi) = (\omega_{bus} - \eta_{bus})\sqrt{|\cos(\pi\Phi(t)/\Phi_0)|} + \eta_{bus}$ with $\Phi(t) = \Phi_p(t)[\sin(\omega_{p1}t) + \sin(\omega_{p2}t + \phi_0)]$ (for simplicity, here $\phi_0 = 0$) and the modulation frequency $\omega_{p1}/2\pi = 2.0$ GHz. Here, similar to Fig. 4(c), raised cosine flat-top pulses are used and the peak modulation amplitude is Φ_p . (a) Population P_{100} (upper panel) and P_{001} (bottom panel) versus the modulation amplitude Φ_p and the modulation frequency ω_{p2} with the qubit prepared in state $|100\rangle$. The ramp time is 15 ns and the total gate length is 100 ns. Dashed orange lines indicate the available regions for realizing \sqrt{iSWAP} gates while the red star is for $iSWAP$ gates. Here, the two-qubit gate is actuated when the difference frequency of the two modulations matches the qubit-qubit detuning. (b) Population P_{101} (upper panel) versus the modulation amplitude Φ_p and the modulation frequency ω_{p2} with the system prepared in state $|101\rangle$. The bottom panel shows the associated conditional phase. The ramp time is 25 ns and the total gate length is 200 ns. Here, the CZ gate is realized when the difference frequency of the two modulations matches the detuning between the energy levels of $|101\rangle$ and $|200\rangle$. Note that discontinuities near the horizontal line at $\Phi_p/\Phi_0 = 0.13$ result from the parasitic interactions between the energy levels of $|101\rangle$ and $|110\rangle$.

TABLE II: Two-qubit schemes with two control pulses. Similar to the qubit addressing, note that for two-qubit gates based on frequency-tunable coupler or bus, static DC flux biases (not listed here) are generally needed for biasing the coupler at their idle points. This can be achieved by using an on-chip programmable magnetic memory, as shown in the left inset of Fig. 3(a).

| Specific | Two-qubit addressing strategy |
|-----------------|--------------------------------------------------------|
| Tunable element | (DT1) Baseband flux pulse + local memory [37]; |
| | (DT2) Two-tone flux modulation; |
| Fixed element | (DF1) Frequency mixer: e.g. three-wave mixing [54–57]; |

qubit gate schemes supporting the row-column addressing:

(DT1) For two fixed-frequency qubits coupled via a coupler (bus), two-qubit gates can be obtained by only tuning the coupler (bus) frequency [78–82]. Given the shared flux pulses, each coupler (bus) can be individually tuned by using the on-chip programmable magnetic memory [30, 31, 37], as shown in Fig. 3(a). Note here that with the help of the local memory, in principle, a single Z line, which is shared by all the couplers or buses, is adequate for performing parallel two-qubit gates.

(DT2) Given the nonlinear dependence of the transmon qubit or transmon coupler frequency on the flux bias, two-qubit gates can be realized by applying two-tone flux modulations on the qubits or the coupler. When the sum or difference frequency of the two-tone modulations match the subharmonic of the qubit-qubit detuning, two-qubit gates can be actuated. For example, considering two fixed-frequency transmon qubits coupled via tunable bus [46], Figure 7 shows two-qubit gates, such as $iSWAP$, \sqrt{iSWAP} , and CZ gates can be obtained by the two-tone modulation of the bus frequency. This two-tone modulation scheme can also be applied to other coupler circuits [47–49]. In Appendix B, we further show that two-qubit gates can be obtained by applying the two-tone flux modulation on one of the two coupled transmon qubits.

(DF1) For two-qubit gates based on driving a single qubit, the three-wave mixer could be used to generate the desired effective single-qubit drive. However, considering the existing techniques [54–57], the strength of the effective drive (here the strength is about ~ 1 MHz) is too weak to support the implementation of a successful, microwave-activated two-qubit gate, such as a cross-resonance (CR) gate [44]. Therefore, here new physical components should be introduced for generating effective drives with large amplitudes.

Given the above discussions, the scheme of (DT2) is more feasible than the other two schemes while the scheme of (DF1) is the most challenging one as new physical components should be demonstrated. Besides the three discussed schemes, similar to the sing-qubit gate scheme of (SF2), two-qubit gates, which are actuated by applying two-tone microwave drives to a qubit or a coupler, should be potential solutions for supporting the row-column addressing and are thus worth exploring in future works.

IV. CHALLENGES TOWARDS LARGE-SCALE MULTIPLEXED CONTROL ARCHITECTURES

In state-of-the-art superconducting quantum processors, several issues, such as distortions of control signals [83, 84], crosstalk between control signals [7], and temporal fluctuations of qubit parameters and coherence times (due to, e.g., two-level systems) [85], are not yet to be well addressed for achieving reliable, accurate quantum computing. This becomes even more challenging within the multiplexed control architecture.

To be more specific, currently, independent control allows various active approaches to be employed for alleviating the detrimental effects of these issues on qubits. On the contrary, due to the control limitations, these approaches cannot be directly applied to the multiplexed control architecture. Thus, rather than attempting to calibrate away these issues, instead, one might turn to fully suppress or eliminate these issues at the qubit chip level. Nevertheless, given state-of-the-art technologies, these progresses are unlikely to be achieved soon. Additionally, at the control pulse level, robust quantum control could be explored to provide resilience against these issues [86], while at the circuit level, gate compilations with adaptations to these issues can be developed [74, 75].

Besides the well-recognized challenges above, there exist two challenges that are particularly important in achieving high-fidelity qubit control with the multiplexed control but are rarely involved in the traditional independent control architecture. In the following, we will discuss the two challenges to be faced when scaling up the multiplexed control architecture.

A. The non-uniformity of qubit parameters

As illustrated in Sec. II and Sec. III, here the gate pulses are shared by multiple qubits, thus the gate condition for each qubit is distinctively intertwined with each other. For clarity, we assume that the coupling efficiencies between control lines and qubits are all the same and focus on the single-qubit gates (similar results can also be obtained for the two-qubit gates discussed in Sec. III B). Thus, for the single-qubit gate scheme illustrated in Sec. III A, given fixed-length drives with the same pulse shape, gates can only be actuated when the gate conditions

$$F(\Omega_i, \Omega_j, \omega_i, \omega_j) = \omega_{ij} \quad (1)$$

are satisfied. Here Ω_i (Ω_j) and ω_i (ω_j) denote the amplitude and frequency of the two drive pulses applied to the qubit, which is located at the intersection of the i th row line and the j th column line. As mentioned in Sec. III A, in the following, we focus on \sqrt{X} gates, which provide more flexibility in setting pulse parameters (similarly, for two-qubit gates, one might prefer \sqrt{CZ} gates [38] or \sqrt{iSWAP} gates, see, e.g., Fig. 7).

Given the condition of Eq. (1) and fixed drive amplitudes, pulse solutions for the scheme, which relies on the resonance condition $f(\omega_i, \omega_j) = \omega_{ij}$ (see, e.g., Fig. 8 in Appendix A), such as (SF2), (ST1), and (ST2), can in principle exist. This is because in a square qubit lattice comprising $n \times n$ qubits, $2n$ different frequencies should be adequate for actuating parallel gate operations. However, even if solutions exist, considering that the resonance conditions are generally intertwined with the drive amplitudes and the non-uniformity of qubit parameters, such as the coupling efficiency between qubits and control lines (i.e., leading to the non-uniformity of the drive amplitude), are ubiquitous in reality, whether and how such solutions can be realized practically in large-scale systems should be open questions and should be an issue worthy of further exploration in further works. In the following, we also consider an alternative approach, i.e., reducing the number of conditions, allowing us to explore another extreme situation.

As shown in Fig. 2(a), in 2D square qubit lattices, the two sets of shared row-column lines allow us to selectively address neighboring qubits, i.e., data qubits and syndrome qubits. In this way, the qubit frequency allocation in each diagonal can follow a zigzag pattern, e.g., data qubits at a frequency band with a typical value of ω_D and syndrome qubits at one another frequency band with a typical value of ω_S . Thus, the gate conditions for data qubits and syndrome qubits are decoupled to each other and we can deal with data qubits and syndrome qubits separately. Accordingly, in the following, we focus on the data qubits, and the gate conditions for data qubits can be approximately reduced to a single one

$$F(\Omega_{D,i}, \Omega_{D,j}, \omega_{D,i}, \omega_{D,j}) = \omega_{D,ij} \simeq \omega_D, \quad (2)$$

where the subscript D denotes the gate condition for data qubits. Finding the solution of the above equation is equivalent to control of an ensemble of qubits, where the qubit frequencies could be different from qubit to qubit (given state-of-the-art technologies [87, 88], the non-uniformity of qubit frequency can be suppressed to the level of 10 MHz [87]), using uniform control pulses, i.e., the parameters of the pulse in each row or column are the same. However, in fact, besides the qubit frequency and the coupling efficiency, the non-uniformity of qubit parameters also results from other factors, such as the qubit anharmonicity and the phase difference among control lines. Therefore, considering all these non-uniformity of qubit parameters, whether one can find the pulse solution of Eq. (2) for multiplexed control of large-scale qubit systems highly hinges on the uniformity of qubit parameters.

As shown in Fig. 3(a), in principle, on-chip programmable magnetic memory can be used to mitigate most of the above-discussed non-uniform issues [30, 37] but its compatibility with high-fidelity qubit control has not yet been demonstrated. Meanwhile, robust quantum control could also be

explored to optimize the control pulse against the remaining non-uniformity issues [86, 89]. Thus, given state-of-the-art quantum technologies and the above discussions, we expect that only taking one of the two types of gate solutions, which supports the gate conditions in Eqs. (1) and (2), alone is challenging to enable high-fidelity multiplexed qubit control at scale. One might choose to take the combination of such two solutions, thus allowing the adaptations to various issues, such as the non-uniformity issue.

B. Gate calibration

While individual gate calibrations and benchmarking can still be possible as in the independent control architecture [90, 91], the multiplexed control should lead to a significant degradation of the efficiency and the performance that can be reached. This is because that the gate calibration procedures for each qubit are intertwined with each other. Alternatively, one might also consider fine-tuning up gates at the quantum circuit level, such as stabilize measurement circuits [92], where the detection events can be used for informing and guiding the optimization of gate parameters.

V. CONCLUSION

In conclusion, we introduce a multiplexed control architecture for superconducting qubits with shared row-column lines, which could in principle provide an efficient approach for parallel controlling N qubits with $O(\sqrt{N})$ control lines. We also propose various single- and two-qubit gate schemes that are both compatible with the row-column qubit addressing and the existing superconducting qubit technologies. Given the inherent parallelism of this architecture, we show that the multiplexed control is suitable for the implementation of structured quantum circuits. As an immediate application, we show that the architecture can be specifically tailored to execute the quantum error correction with surface code. We envision that a small-scale demonstration of the multiplexed qubit control could be feasible with the current technologies and hope that our work could motivate further experimental and theoretical research in incorporating shared control into scalable quantum information processing with superconducting qubits.

Acknowledgments

The author would like to thank Guangming Xue, Jun Li, Kunzhe Dai, Zhiyun Han, and Fei Yan for the insightful discussions. Thanks also go to Peng Xu, Dong Lan, and Haifeng Yu for their generous support. The author also gratefully acknowledges support from the National Natural Science Foundation of China (Grants No.12204050) and the Beijing Academy of Quantum Information Sciences.

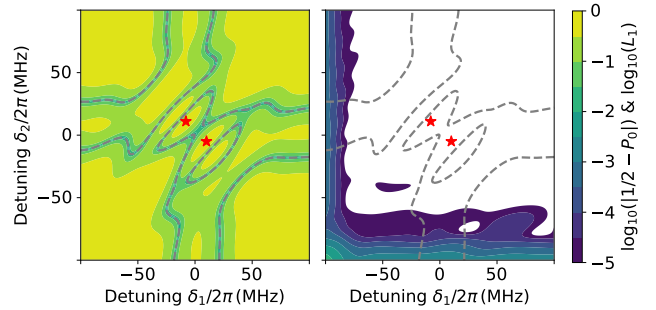


FIG. 8: Nonlinear dependence on the frequency difference of the two-tone microwave drive. The left (right) panel shows the population P_0 (the leakage L_1) versus the drive-qubit detunings δ_1 and δ_2 (white regions are where leakage below 10^{-5}). As in Fig. 3, the qubit frequency and the anharmonicity are $\omega_q/2\pi = 5.25$ GHz and $\eta_q/2\pi = -250$ MHz, respectively. Here, the peak drive parameters are $\Omega_{1(2)}/2\pi = 25$ MHz. Dashed grey lines indicate the available regions for realizing \sqrt{X} gates while the red star is for X gates

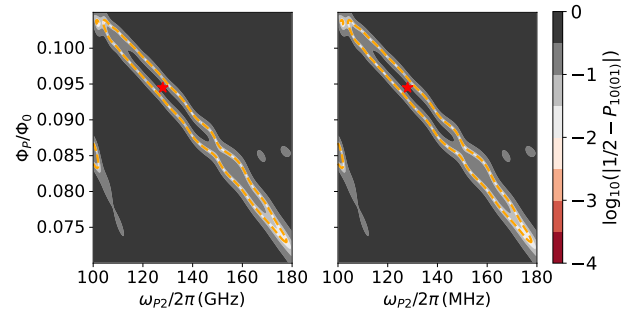


FIG. 9: The two-qubit gate operations based on applying two-tone flux modulations to qubits. We consider that two transmon qubits (labeled by Q_a and Q_b) are coupled directly and a two-tone flux modulation is applied to the frequency-tunable qubit Q_a . The system state is denoted by $|Q_a Q_b\rangle$. Here, as in Fig. 7(a), the raised cosine flat-top pulses are used with a total gate length of 100 ns and a ramp time of 15 ns. The left (right) panel shows population P_{10} (P_{01}) versus the modulation amplitude Φ_p and the modulation frequency ω_{p2} with the system prepared in state $|10\rangle$. Dashed orange lines indicate the available regions for realizing $\sqrt{i\text{SWAP}}$ gates while the red star is for $i\text{SWAP}$ gates.

Appendix A: Nonlinear dependence on the frequency difference in the two-tone drive scheme

For the two-tone microwave drives studied in Fig. 3(d), Figure 8 shows the population P_0 and the leakage L_1 versus the drive-qubit detunings δ_1 and δ_2 .

Appendix B: iswap gates using two-tone flux modulation of qubits

Here, we consider that one frequency-tunable transmon qubit (labeled by Q_a) is coupled fixedly to a fixed-frequency transmon qubit (labeled by Q_b) with the coupling strength of $g/2\pi = 5.5$ MHz. The qubit frequencies and the qubit anharmonicities are $\omega_{a(b)}/2\pi = 5.05(5.25)$ GHz and $\eta_{a(b)}/2\pi =$

250 MHz, respectively. When applying the two-tone flux modulation to Q_a , the qubit frequency is approximated by $\omega_a(\Phi) = (\omega_a - \eta_a)\sqrt{|\cos(\pi\Phi(t)/\Phi_0)|} + \eta_a$ with $\Phi(t) = \Phi_p(t)[\sin(\omega_{p1}t) + \sin(\omega_{p2}t + \phi_0)]$. Here, the modulation frequency $\omega_{p1}/2\pi = 50$ MHz and $\phi_0 = 0$ for simplicity. Figure 9 shows that under such a two-tone flux modulation, two-qubit gates, such as $\sqrt{i}\text{SWAP}$ gates and iSWAP gates, can be actuated.

[1] B. M. Terhal, Quantum Error Correction for Quantum Memories, *Rev. Mod. Phys.* **87**, 307 (2015).

[2] E. Dennis, A. Kitaev, A. Landahl, and J. Preskill, Topological quantum memory, *J. Math. Phys.* **43**, 4452-4505 (2002).

[3] E. Campbell, A series of fast-paced advances in Quantum Error Correction, *Nat. Rev. Phys.* (2024).

[4] S. Krinner, N. Lacroix, A. Remm, A. D. Paolo, E. Genois, C. Leroux, C. Hellings, S. Lazar, F. Swiadek, J. Herrmann, G. J. Norris, C. K. Andersen, M. Müller, A. Blais, C. Eichler, and A. Wallraff, Realizing repeated quantum error correction in a distance-three surface code, *Nature* **605**, 669-674 (2022).

[5] Y. Zhao, Y. Ye, H.-L. Huang, Y. Zhang, D. Wu, H. Guan, Q. Zhu, Z. Wei, T. He, S. Cao *et al.*, Realization of an Error-Correcting Surface Code with Superconducting Qubits, *Phys. Rev. Lett.* **129**, 030501 (2022).

[6] N. Sundaresan, T. J. Yoder, Y. Kim, M. Li, E. H. Chen, G. Harper, T. Thorbeck, A. W. Cross, A. D. Córcoles, and M. Takita, Demonstrating multi-round subsystem quantum error correction using matching and maximum likelihood decoders, *Nat. Commun.* **14**, 2852 (2023).

[7] Q. Acharya, I. Aleiner, R. Allen, T. I. Andersen, M. Ansmann, F. Arute, K. Arya, A. Asfaw, J. Atalaya, R. Babbush *et al.*, Suppressing Quantum Errors by Scaling a Surface Code Logical Qubit, *Nature (London)* **614**, 676 (2023).

[8] A. G. Fowler, M. Mariantoni, J. M. Martinis, and A. N. Cleland, Surface codes: Towards practical large-scale quantum computation, *Phys. Rev. A* **86**, 032324 (2012).

[9] A. Gidney and M. Ekerå, How to factor 2048 bit RSA integers in 8 hours using 20 million noisy qubits, *Quantum* **5**, 433 (2021).

[10] Z. Chen, Metrology of Quantum Control and Measurement in Superconducting Qubits, Ph.D. thesis. University of California, Santa Barbara, 2018.

[11] S. Krinner, S. Storz, P. Kurpiers, P. Magnard, J. Heinsoo, R. Keller, J. Lütolf, C. Eichler, and A. Wallraff, Engineering cryogenic setups for 100-qubit scale superconducting circuit systems, *EPJ Quantum Technology* **6**, 2 (2019).

[12] P. Krantz, M. Kjaergaard, F. Yan, T. P. Orlando, S. Gustavsson, and W. D. Oliver, A Quantum Engineer's Guide to Superconducting Qubits, *Appl. Phys. Rev.* **6**, 021318 (2019).

[13] D. P. Franke, J. S. Clarkeb, L. M. K. Vandersypenab, and M. Veldhorsta, Rent's rule and extensibility in quantum computing, *Microprocess. Microsys.* **67**, 1 (2019).

[14] L. M. K. Vandersypen, H. Bluhm, J. S. Clarke, A. S. Dzurak, R. Ishihara, A. Morello, D. J. Reilly, L. R. Schreiber, and M. Veldhorst, Interfacing spin qubits in quantum dots and donors: hot, dense, and coherent, *npj Quantum Inf.* **3**, 34 (2017).

[15] D. J. Reilly, Challenges in Scaling-up the Control Interface of a Quantum Computer, *2019 IEEE International Electron Devices Meeting (IEDM)*, 31.7 (2019).

[16] J. M. Martinis, Information Constraints for Scalable Control in a Quantum Computer, [arXiv:2012.14270](https://arxiv.org/abs/2012.14270).

[17] S. Asaad, C. Dickel, S. Poletto, A. Bruno, N. K. Langford, M. A. Rol, D. Deurloo, and L. DiCarlo, Independent, extensible control of same-frequency superconducting qubits by selective broadcasting, *npj Quantum Inf.* **2**, 16029 (2016).

[18] F. Lecocq, F. Quinlan, K. Cicak, J. Aumentado, S. A. Diddams, and J. D. Teufel, Control and readout of a superconducting qubit using a photonic link, *Nature* **591**, 575-579 (2021).

[19] R. McDermott, M. G. Vavilov, B. L. T. Plourde, F. K. Wilhelm, P. J. Liebermann, O. A. Mukhanov, and T. A. Ohki, Quantum-classical interface based on single flux quantum digital logic, *Quantum Sci. Technol.* **3**, 024004 (2018).

[20] J. C. Bardin, E. Jeffrey, E. Lucero, T. Huang, S. Das, D. T. Sank, O. Naaman, A. E. Megrant, R. Barends, T. White *et al.*, Design and Characterization of a 28-nm Bulk-CMOS Cryogenic Quantum Controller Dissipating Less Than 2 mW at 3 K, *IEEE Journal of Solid-State Circuits* **54**, 3043 (2019).

[21] J. P. G. Van Dijk, B. Patra, S. Subramanian, X. Xue, N. Samkharadze, A. Corna, C. Jeon, F. Sheikh, E. Juarez-Hernandez, B. P. Esparza *et al.*, A scalable cryoCMOS controller for the wideband frequency-multiplexed control of spin qubits and transmons, *IEEE Journal of Solid-State Circuits* **55**, 2930 (2020).

[22] S. Chakraborty, D. J. Frank, K. Tien, P. Rosno, M. Yeck, J. A. Glick, R. Robertazzi, R. Richetta, J. F. Bulzacchelli, D. Underwood *et al.*, A cryo-CMOS low-power semi-autonomous transmon qubit state controller in 14-nm FinFET technology, *IEEE Journal of Solid-State Circuits* **57**, 3258 (2022).

[23] N. Takeuchi, T. Yamae, W. Luo, F. Hirayama, T. Yamamoto, and N. Yoshikawa, Scalable flux controllers using adiabatic superconductor logic for quantum processors, *Phys. Rev. Research* **5**, 013145 (2023).

[24] N. Takeuchi, T. Yamae, T. Yamashita, T. Yamamoto, and N. Yoshikawa, Scalable quantum-bit controller using adiabatic superconductor logic, [arXiv:2310.06544](https://arxiv.org/abs/2310.06544).

[25] R. Acharya, S. Brebels, A. Grill, J. Verjauw, Ts. Ivanov, D. Perez Lozano, D. Wan, J. Van Damme, A. M. Vadiraj, M. Mongillo, B. Govoreanu, J. Craninckx, I. P. Radu, K. De Greve, G. Gielen, F. Catthoor, and A. Potočnik, Multiplexed superconducting qubit control at millikelvin temperatures with a low-power cryoCMOS multiplexer, *Nat. Electron.* **6**, 900-909 (2023).

[26] C.H. Liu, A. Ballard, D. Olaya, D.R. Schmidt, J. Biesecker, T. Lucas, J. Ullom, S. Patel, O. Rafferty, A. Opremcak, K. Dodge, V. Iaia, T. McBroom, J.L. DuBois, P.F. Hopkins, S.P. Benz, B.L.T. Plourde, and R. McDermott, Single Flux Quantum-Based Digital Control of Superconducting Qubits in a Multi-chip Module, *PRX Quantum* **4**, 030310 (2023).

[27] C. D. Hill, E. Peretz, S. J. Hile, M. G. House, M. Fuechsle,

S Rogge, M. Y. Simmons, and L. C. L. Hollenberg, A surface code quantum computer in silicon, *Sci. Adv.* **1**, e1500707 (2015).

[28] M. Veldhorst, H. G. J. Eenink, C. H. Yang, and A. S. Dzurak, Silicon CMOS architecture for a spin-based quantum computer, *Nat. Commun.* **8**, 1766 (2017).

[29] R. Li, L. Petit, D. P. Franke, J. P. Dehollain, J. Helsen, M. Steudtner, N. K. Thomas, Z. R. Yoscovits, K. J. Singh, S. Wehner *et al.*, A Crossbar Network for Silicon Quantum Dot Qubits, *Sci. Adv.* **4**, eaar3960 (2018).

[30] M. W. Johnson, P. Bunyk, F. Maibaum, E. Tolkacheva, A. J. Berkley, E. M. Chapple, R. Harris, J. Johansson, T. Lanting, and I. Perminov *et al.*, A Scalable Control System for a Superconducting Adiabatic Quantum Optimization Processor, *Supercond. Sci. Technol.* **23**, 065004 (2010).

[31] P. I. Bunyk, E. M. Hoskinson, M. W. Johnson, E. Tolkacheva, F. Altomare, A. J. Berkley, R. Harris, J. P. Hilton, T. Lanting, A. J. Przybysz *et al.*, Architectural considerations in the design of a superconducting quantum annealing processor, *IEEE Trans. Appl. Supercond.* **24**, 1700110 (2014).

[32] M. Jerger, S. Poletto, P. Macha, U. Hübner, A. Lukashenko, E. Il'ichev, and A. V. Ustinov, Readout of a qubit array via a single transmission line, *Europhys. Lett.* **96**, 40012 (2011).

[33] M. Jerger, S. Poletto, P. Macha, U. Hübner, E. Il'ichev, and A. V. Ustinov, Frequency division multiplexing readout and simultaneous manipulation of an array of flux qubits, *Appl. Phys. Lett.* **101**, 042604 (2012).

[34] Y. Chen, D. Sank, P. O'Malley, T. White, R. Barends, B. Chiaro, J. Kelly, E. Lucero, M. Mariantoni, A. Megrant, C. Neill, A. Vainsencher, J. Wenner, Y. Yin, A. N. Cleland, and John M. Martinis, Multiplexed dispersive readout of superconducting phase qubits, *Appl. Phys. Lett.* **101**, 182601 (2012).

[35] D.-Y. Li, J. Chu, W. Zheng, D. Lan, J. Zhao, S.-X. Li, X.-S. Tan, and Y. Yu, Universal quantum control based on parametric modulation in superconducting circuits, *Chin. Phys. B* **30**, 070308 (2021).

[36] J. H. Béjanin, C. T. Earnest, and M. Mariantoni, The Quantum Socket and DemuXYZ-Based Gates with Superconducting Qubits, [arXiv:2211.00143](https://arxiv.org/abs/2211.00143).

[37] P. Zhao, R. Wang, M.-J. Hu, T. Ma, P. Xu, Y. Jin, and H. Yu, Baseband Control of Superconducting Qubits with Shared Microwave Drives, *Phys. Rev. Appl.* **19**, 054050 (2023).

[38] P. Shi, J. Yuan, F. Yan, and H. Yu, Multiplexed control scheme for scalable quantum information processing with superconducting qubits, [arXiv:2312.06911](https://arxiv.org/abs/2312.06911).

[39] Z. György, A. Pályi, and G. Széchenyi, Electrically driven spin resonance with bichromatic driving, *Phys. Rev. B* **106**, 155412 (2022).

[40] S. Bosco, S. Geyer, L. C. Camenzind, R. S. Eggli, A. Fuhrer, R. J. Warburton, D. M. Zumbühl, J. C. Egues, A. V. Kuhlmann, and D. Loss, Phase driving hole spin qubits, [arXiv:2303.03350](https://arxiv.org/abs/2303.03350).

[41] V. John, F. Borsoi, Z. György, C.-A. Wang, G. Széchenyi, F. v. Riggelen, W. I. L. Lawrie, N. W. Hendrickx, A. Sammak, G. Scappucci, A. Pályi, and M. Veldhorst, Bichromatic Rabi control of semiconductor qubits, [arXiv:2308.01720](https://arxiv.org/abs/2308.01720).

[42] Z. Han, C. Lyu, Y. Zhou, J. Yuan, J. Chu, W. Nuerbolati, H. Jia, L. Nie, W. Wei, Z. Yang *et al.*, Multilevel variational spectroscopy using a programmable quantum simulator, *Phys. Rev. Research* **6**, 013015 (2024).

[43] D. C. McKay, C. J. Wood, S. Sheldon, J. M. Chow, and J. M. Gambetta, Efficient Z gates for quantum computing, *Phys. Rev. A* **96**, 022330 (2017).

[44] J. M. Chow, A. D. Córcoles, J. M. Gambetta, C. Rigetti, B. R. Johnson, J. A. Smolin, J. R. Rozen, G. A. Keefe, M. B. Rothwell, M. B. Ketchen, and M. Steffen, Simple All-Microwave Entangling Gate for Fixed-Frequency Superconducting Qubits, *Phys. Rev. Lett.* **107**, 080502 (2011).

[45] S. A. Caldwell, N. Didier, C. A. Ryan, E. A. Sete, A. Hudson, P. Karalekas, R. Manenti, M. P. da Silva, R. Sinclair, E. Acalá *et al.*, Parametrically Activated Entangling Gates Using Transmon Qubits, *Phys. Rev. Appl.* **10**, 034050 (2018).

[46] D. C. McKay, S. Filipp, A. Mezzacapo, E. Magesan, J. M. Chow, and J. M. Gambetta, Universal gate for fixed-frequency qubits via a tunable bus, *Phys. Rev. Applied* **6**, 064007 (2016).

[47] P. S. Mundada, G. Zhang, T. Hazard, and A. A. Houck, Suppression of Qubit Crosstalk in a Tunable Coupling Superconducting Circuit, *Phys. Rev. Applied* **12**, 054023 (2019).

[48] X. Y. Han, T. Q. Cai, X. G. Li, Y. K. Wu, Y. W. Ma, Y. L. Ma, J. H. Wang, H. Y. Zhang, Y. P. Song, and L. M. Duan, Error analysis in suppression of unwanted qubit interactions for a parametric gate in a tunable superconducting circuit, *Phys. Rev. A* **102**, 022619 (2020).

[49] K. Kubo and H. Goto, Fast parametric two-qubit gate for highly detuned fixed-frequency superconducting qubits using a double-transmon coupler, *Appl. Phys. Lett.* **122**, 064001 (2023).

[50] C. Horsman, A. G. Fowler, S. Devitt, and R. V. Meter, Surface code quantum computing by lattice surgery, *New J. Phys.* **14**, 123011 (2012).

[51] A. G. Fowler and C. Gidney, Low overhead quantum computation using lattice surgery, [arXiv:1808.06709](https://arxiv.org/abs/1808.06709).

[52] J. Koch, T. M. Yu, J. Gambetta, A. A. Houck, D. I. Schuster, J. Majer, A. Blais, M. H. Devoret, S. M. Girvin, and R. J. Schoelkopf, Charge-insensitive qubit design derived from the cooper pair box, *Phys. Rev. A* **76**, 042319 (2007).

[53] V. E. Manucharyan, J. Koch, L. I. Glazman, and M. H. Devoret, Fluxonium: Single Cooper-pair circuit free of charge offsets, *Science* **326**, 113 (2009).

[54] N. E. Frattini, U. Vool, S. Shankar, A. Narla, K. M. Sliwa, and M. H. Devore, 3-wave mixing Josephson dipole element, *Appl. Phys. Lett.* **110**, 222603 (2017).

[55] B. J. Chapman, S. J. de Graaf, S. H. Xue, Y. Zhang, J. Teoh, J. C. Curtis, T. Tsunoda, A. Eickbusch, A. P. Read, A. Kottandavida, S. O. Mundhada, L. Frunzio, M. H. Devoret, S. M. Girvin, and R. J. Schoelkopf, High-On-Off-Ratio Beam-Splitter Interaction for Gates on Bosonically Encoded Qubits, *PRX Quantum* **4**, 020355 (2023).

[56] Yu-xi Liu, H.-C. Sun, Z. H. Peng, A. Miranowicz, J. S. Tsai, and F. Nori, Controllable microwave three-wave mixing via a single three-level superconducting quantum circuit, *Sci Rep* **4**, 7289 (2014).

[57] P. Zhao, Z. Jin, P. Xu, X. Tan, H. Yu, and Y. Yu, Two-Photon Driven Kerr Resonator for Quantum Annealing with Three-Dimensional Circuit QED, *Phys. Rev. Appl.* **10**, 024019 (2018).

[58] K. Dai, H. Wu, P. Zhao, M. Li, Q. Liu, G. Xue, X. Tan, H. Yu, and Y. Yu, Quantum simulation of the general semi-classical Rabi model in regimes of arbitrarily strong driving, *Appl. Phys. Lett.* **111**, 242601 (2017).

[59] Y.-M. He, H. Wang, C. Wang, M.-C. Chen, X. Ding, J. Qin, Z.-C. Duan, S. Chen, J.-P. Li, R.-Z. Liu *et al.*, Coherently driving a single quantum two-level system with dichromatic laser pulses, *Nat. Phys.* **15**, 941 (2019).

[60] Z. X. Koong, E. Scerri, M. Rambach, M. Cygorek, M. BrotonsGisbert, R. Picard, Y. Ma, S. I. Park, J. D. Song, E. M. Gauger, and B. D. Gerardot, Coherent Dynamics in Quantum Emitters under Dichromatic Excitation, *Phys. Rev. Lett.* **126**, 047403 (2021).

[61] T. K. Bracht, M. Cosacchi, T. Seidelmann, M. Cygorek, A.

Vagov, V. M. Axt, T. Heindel, and D. E. Reiter, Swing-Up of Quantum Emitter Population Using Detuned Pulses, [PRX Quantum](#) **2**, 040354 (2021).

[62] Z. T. Wang, P. Zhao, Z. H. Yang, Ye Tian, H. F. Yu, and S. P. Zhao, Escaping Detrimental Interactions with Microwave-Dressed Transmon Qubits, [Chin. Phys. Lett.](#) **40**, 070304 (2023).

[63] F. Motzoi, J. M. Gambetta, P. Rebentrost, and F. K. Wilhelm, Simple Pulses for Elimination of Leakage in Weakly Nonlinear Qubits, [Phys. Rev. Lett.](#) **103**, 110501 (2009).

[64] Z. Chen, J. Kelly, C. Quintana, R. Barends, B. Campbell, Y. Chen, B. Chiaro, A. Dunsworth, A. G. Fowler, E. Lucero, E. Jeffrey, A. Megrant, J. Mutus, M. Neeley, C. Neill, P. J. J. O'Malley, P. Roushan, D. Sank, A. Vainsencher, J. Wenner, T. C. White, A. N. Korotkov, and J. M. Martinis, Measuring and Suppressing Quantum State Leakage in a Superconducting Qubit, [Phys. Rev. Lett.](#) **116**, 020501 (2016).

[65] R. Harris, T. Lanting, A. J. Berkley, J. Johansson, M. W. Johnson, P. Bunyk, E. Ladizinsky, N. Ladizinsky, T. Oh, and S. Han, Compound Josephson-junction coupler for flux qubits with minimal crosstalk, [Phys. Rev. B](#) **80**, 052506 (2009).

[66] Alec Maassen van den Brink, A. J. Berkley, and M. Yalowsky, Mediated tunable coupling of flux qubits, [New J. Phys.](#) **7**, 230 (2005).

[67] R. Harris, A. J. Berkley, M. W. Johnson, P. Bunyk, S. Govorkov, M. C. Thom, S. Uchaikin, A. B. Wilson, J. Chung, E. Holtham, J. D. Biamonte, A. Yu. Smirnov, M. H. S. Amin, and Alec Maassen van den Brink, Sign- and Magnitude-Tunable Coupler for Superconducting Flux Qubits, [Phys. Rev. Lett.](#) **98**, 177001 (2007).

[68] J. D. Strand, Matthew Ware, F. Beaudoin, T. A. Ohki, B. R. Johnson, A. Blais, and B. L. T. Plourde, First-order sideband transitions with flux-driven asymmetric transmon qubits, [Phys. Rev. B](#) **87**, 220505(R) (2013).

[69] P. Zhao, T. Ma, Y. Jin, and H. Yu, Combating fluctuations in relaxation times of fixed-frequency transmon qubits with microwave-dressed states, [Phys. Rev. A](#) **105**, 062605 (2022).

[70] T. K. Bracht, T. Seidelmann, Y. Karli, F. Kappe, V. Remesh, G. Weihs, V. M. Axt, and D. E. Reiter, Dressed-state analysis of two-color excitation schemes, [Phys. Rev. B](#) **107**, 035425 (2023).

[71] I. Zuk, D. Cohen, A. V. Gorshkov, and A. Retzker, Robust gates with spin-locked superconducting qubits, [arXiv:2306.09149](#).

[72] C. J. Wood and J. M. Gambetta, Quantification and characterization of leakage errors, [Phys. Rev. A](#) **97**, 032306 (2018).

[73] J. Chen, D. Ding, C. Huang, and Q. Ye, Compiling arbitrary single-qubit gates via the phase shifts of microwave pulses, [Phys. Rev. Research](#) **5**, L022031 (2023).

[74] R. Wang, P. Zhao, Y. Jin, and H. Yu, Control and mitigation of microwave crosstalk effect with superconducting qubits, [Appl. Phys. Lett.](#) **121**, 152602 (2022).

[75] R. Wang, P. Zhao, and H. Yu, Universality of universal single-qubit-gate decomposition with coherent errors, [arXiv:2211.00365](#).

[76] K. X. Wei, E. Pritchett, D. M. Zajac, D.C. McKay, and S. Merkel, Characterizing non-Markovian Off-Resonant Errors in Quantum Gates, [arXiv:2302.10881](#).

[77] L. H. Pedersen, N. M. Møller, and K. Mølmer, Fidelity of quantum operations, [Phys. Lett. A](#) **367**, 47 (2007).

[78] M. C. Collodo, J. Herrmann, N. Lacroix, C. K. Andersen, A. Remm, S. Lazar, J. Besse, T. Walter, A. Wallraff, and C. Eichler, Implementation of Conditional Phase Gates Based on Tunable $Z\bar{Z}$ Interactions, [Phys. Rev. Lett.](#) **125**, 240502 (2020).

[79] Y. Xu, J. Chu, J. Yuan, J. Qiu, Y. Zhou, L. Zhang, X. Tan, Y. Yu, S. Liu, J. Li, F. Yan, and D. Yu, High-Fidelity, High-Scalability Two-Qubit Gate Scheme for Superconducting Qubits, [Phys. Rev. Lett.](#) **125**, 240503 (2020).

[80] P. Zhao, K. Linghu, Z. Li, P. Xu, R. Wang, G. Xue, Y. Jin, and H. Yu, Quantum Crosstalk Analysis for Simultaneous Gate Operations on Superconducting Qubits, [PRX Quantum](#) **3**, 020301 (2022).

[81] H. Goto, Double-Transmon Coupler: Fast Two-Qubit Gate with No Residual Coupling for Highly Detuned Superconducting Qubits, [Phys. Rev. Appl.](#) **18**, 034038 (2022).

[82] D. L. Campbell, A. a Kamal, L. Ranzani, M. Senatore, and M. D. LaHaye, Modular Tunable Coupler for Superconducting Circuits, [Phys. Rev. Appl.](#) **19**, 064043 (2023).

[83] R. Barends, J. Kelly, A. Megrant, A. Veitia, D. Sank, E. Jeffrey, T. C. White, J. Mutus, A. G. Fowler, B. Campbell *et al.*, Superconducting quantum circuits at the surface code threshold for fault tolerance, [Nature](#) **508**, 500 (2014).

[84] S. Gustavsson, O. Zwier, J. Bylander, F. Yan, F. Yoshihara, Y. Nakamura, T. P. Orlando, and W. D. Oliver, Improving Quantum Gate Fidelities by Using a Qubit to Measure Microwave Pulse Distortions, [Phys. Rev. Lett.](#) **110**, 040502 (2013).

[85] C. Müller, J. H. Cole, and J. Lisenfeld, Towards understanding two-level-systems in amorphous solids: insights from quantum circuits, [Rep. Prog. Phys.](#) **82**, 124501 (2019).

[86] D. Dong and I. R. Petersen, Quantum control theory and applications: a survey, [IET Control. Theory Appl.](#) **4**, 2651 (2010).

[87] J. B. Hertzberg, E. J. Zhang, S. Rosenblatt, E. Magesan, J. A. Smolin, J.-B. Yau, V. P. Adiga, M. Sandberg, M. Brink, J. M. Chow, and J. S. Orcutt, Laser-annealing Josephson junctions for yielding scaled-up superconducting quantum processors, [npj Quantum Inf.](#) **7**, 129 (2021).

[88] D. P. Pappas, M. Field, C. Kopas, J. A. Howard, X. Wang, E. Lachman, L. Zhou, J. Oh, K. Yadavalli, E. A. Sete, A. Bestwick, M. J. Kramer, and J. Y. Mutus, Alternating Bias Assisted Annealing of Amorphous Oxide Tunnel Junctions, [arXiv:2401.07415](#).

[89] B. Shao, X. Yang, R. Liu, Y. Zhai, D. Lu, T. Xin, and J. Li, Multiple Classical Noise Mitigation by Multiobjective Robust Quantum Optimal Control, [arXiv:2403.00298](#).

[90] J. Kelly, P. O'Malley, M. Neeley, H. Neven, and J. M. Martinis, Physical qubit calibration on a directed acyclic graph, [arXiv:1803.03226](#).

[91] P. V. Klimov, J. Kelly, J. M. Martinis, and H. Neven, The snake optimizer for learning quantum processor control parameters, [arXiv:2006.04594](#).

[92] J. Kelly, R. Barends, A. G. Fowler, A. Megrant, E. Jeffrey, T. C. White, D. Sank, J. Y. Mutus, B. Campbell, Yu Chen, Z. Chen, B. Chiaro, A. Dunsworth, E. Lucero, M. Neeley, C. Neill, P. J. J. O'Malley, C. Quintana, P. Roushan, A. Vainsencher, J. Wenner, and John M. Martinis, Scalable *in situ* qubit calibration during repetitive error detection, [Phys. Rev. A](#) **94**, 032321 (2016).